CMC-citric acid Cu(II) cross-linked binder approach to improve the electrochemical performance of Si-based electrodes

D. Mazouzi, R. Grissa, M. Paris, Z. Karkar, L. Huet, D. Guyomard, L. Roué, T. Devic, B. Lestriez

▶ **To cite this version:**

D. Mazouzi, R. Grissa, M. Paris, Z. Karkar, L. Huet, et al.. CMC-citric acid Cu(II) cross-linked binder approach to improve the electrochemical performance of Si-based electrodes. Electrochimica Acta, 2019, 304, pp.495-504. 10.1016/j.electacta.2019.03.026 . hal-02090713

HAL Id: hal-02090713
https://hal.science/hal-02090713

Submitted on 22 Oct 2021

HAL is a multi-disciplinary open access archive for the deposit and dissemination of scientific research documents, whether they are published or not. The documents may come from teaching and research institutions in France or abroad, or from public or private research centers.

L'archive ouverte pluridisciplinaire **HAL**, est destinée au dépôt et à la diffusion de documents scientifiques de niveau recherche, publiés ou non, émanant des établissements d'enseignement et de recherche français ou étrangers, des laboratoires publics ou privés.

Distributed under a Creative Commons Attribution - NonCommercial 4.0 International License

Version of Record: https://www.sciencedirect.com/science/article/pii/S0013468619304207
Manuscript_e253f150fc1f2f4057849bddbab1080f

CMC-citric acid Cu(II) cross-linked binder approach to improve the electrochemical performance of Si-based electrodes

D. Mazouzi,[a] R. Grissa,[b] M. Paris,[b] Z. Karkar,[c] L. Huet,[b,c] D. Guyomard,[b] L. Roué,[c] T. Devic,[b] B. Lestriez[b]*

a *Materials, Natural Substances, Environment and Modeling Laboratory. Multidisciplinary Faculty of Taza. University of Sidi Mohamed Ben Abdellah, Fes, Morocco.*

[b] *Institut des Matériaux Jean Rouxel (IMN), Université de Nantes, CNRS UMR 6502, 2 rue de la Houssinière, BP 32229, 44322 Nantes cedex 3, France.*

[c] *Institut National de la Recherche Scientifique (INRS), Centre Énergie, Matériaux, Télécommunications (EMT), 1650, Boulevard Lionel Boulet, Varennes, QC J3X 1S2, Canada.*

* bernard.lestriez@cnrs-imn.fr

Abstract

Maturation, which consists of storing the electrode under humid atmosphere before drying and cell assembly, improves very significantly the cyclability of silicon-based composite electrodes made with an acidic binder. During maturation, the atmospheric-induced corrosion of the current collector releases oxidized copper species that migrate into the electrode to physically crosslink the binder phase, substantially modifying its resiliency to the silicon volume variation. The pre-addition of a small amount of copper salt in the electrode slurry allows to reach similar improvement of electrochemical performance than maturation.

Keywords: silicon; carboxymethyl cellulose; citric acid, copper; coordination chemistry

1. Introduction

The use of silicon as negative electrode active material in Li-ion batteries could significantly increase their energy density compared to commercial ones based on graphite. However, several difficulties associated with the strong volume expansion and contraction of the active material during its lithiation and delithiation have prevented their implementation in commercial batteries. [1] Indeed, these volume variations cause the passivation layer formed on the surface of the active material (the solid-electrolyte interphase (SEI)) to rupture, leading at each cycle to additional degradation of the electrolyte on the reducing surface of lithiated silicon. Moreover, these volume variations lead more or less rapidly during cycling to a mechanical failure (loss of cohesion/adhesion) of the electrodes and a drop in capacity. For many years and until very recently, many studies have been carried out and have led to significant progress in understanding these problems and in the way to solve them at least

© 2019 published by Elsevier. This manuscript is made available under the CC BY NC user license
https://creativecommons.org/licenses/by-nc/4.0/

partially, thanks to new materials, additives for electrolytes, binders and conducting additives for electrode formulation optimization. [2-7]

Polymeric binders play an active role in maintaining the electrode morphology and in helping to stabilize cracked silicon particles along with the SEI layer. [8-12] The first class of suitable binders for silicon-based electrodes are natural and/or water soluble. They possess polar groups (e.g. –COOH, -OH, $-NH_2$) able to strongly interact with or chemically graft to the active particle surface through hydrogen or covalent bonds. They are able to maintain a good level of mechanical strength when soaked in the liquid electrolyte. They have good film-forming ability to deposit as conformal coating at the surface of the silicon particles and possess acceptable Li^+ conductivity (thanks to the presence of polar groups) to work as protective artificial SEI. [13] Self-healing property, based on strong but noncovalent binder–binder and binder–silicon particles supramolecular interactions, such as ion-dipole and hydrogen interactions, is considered as mandatory for durable cycling because these interactions are permanently stressed by the silicon volume expansion and contraction. [14] Finally, ramified or cross-linked macromolecular architectures are considered superior to linear ones because the presence of numerous ramifications shall result in superior adhesion and cohesion strength. [11] The second class of suitable binders are aromatic ones (including electronically conductive polymers). Their *in situ* electrochemical reduction lead to a hydrogen containing carbon coating around the silicon particles, reducing electrolyte decomposition and improving electronic contact. [7]

Whatever the binder type, the size and the shape of the carbon conductive additives are important to level the mechanical stress within the stacking of particles. The processing conditions of the electrode slurry plays a lot on the homogeneity in the distribution of the different materials and thus on the efficiency of the binder and the carbon additive. Finally, the interface with the copper current collector can be designed through chemical or mechanical treatments to increase the adhesion with the electrode. [8]

We recently discovered a simple post-processing treatment that improves very significantly the mechanical strength and the cyclability of silicon-based composite electrodes made with an acidic linear non-aromatic aqueous binder. This treatment, called maturation, consists of storing the electrode under humid atmosphere (about 80% relative humidity (RH)) for at least 2–3 days before drying and cell assembly. [15,16] Compared to a standard (non-matured) electrode, a matured electrode shows: *(i)* in its pristine and dry states, a significantly higher hardness, peel and scratch resistance, and *(ii)* upon electrochemical cycling, a much

better resistance to cracking and delamination from the current collector, lower and more reversible volume expansion. [17]

The effectiveness of this maturation treatment was observed for negative electrodes made with various silicon powders and for binders bearing carboxylic functional groups, either carboxymethyl cellulose (CMC) mixed with citric acid (CA) or polyacrylic acid (PAA). The effectiveness of maturation was also observed with respect to the calendering of silicon-based electrodes. Calendering is essential to achieve a high volume fraction of active material, and a high coating volumetric capacity. [18] However, this mechanical treatment is observed to deteriorate the mechanical strength of the electrode, likely by degrading the bonds between the binder and/or the current collector surface or the binder itself, inducing a decrease of the cycling stability. If applied as a post-calendering treatment, the maturation step restores and even improves the mechanical strength of the electrode, which makes possible to cycle calendered electrodes with high active mass loading and low porosity. [19]

The improvement of the electrode cohesion with maturation was attributed to the fortification of the binder connections between silicon particles, as a result of some dewetting of the binder layer adsorbed on the free surface of the silicon particles to concentrate at the contact points between silicon particles. The improvement of the electrode adhesion to the copper current collector was attributed to the formation of copper-carboxylate coordination bonds between the current collector and the electrode binder, as a result of an atmospheric-induced corrosion of copper activated by the acidic functional groups of the binder. [16]

In this follow-up study, a better understanding of the maturation process is achieved. In particular, the critical role of the atmospheric-induced corrosion of the current collector is addressed. It is discovered that oxidized copper species can migrate into the electrode to physically crosslink the binder phase through the formation of copper carboxylate coordination bonds. Very interestingly, the pre-addition of a small amount of copper salt in the electrode slurry allows to reach similar level of performance improvement than maturation, but without the need of exposing the electrode for several days to humid atmosphere.

2. Experimental

2.1 Materials

Ball-milled Si powder was used as active material. Si powder (99.999%, 20 mesh, Materion) was loaded and sealed under argon atmosphere into a 55 ml stainless-steel vial containing two 11.1 mm/5.4 g and one 14.3 mm/11.5 g diameter/mass stainless-steel balls. The ball-to-powder mass ratio was 5:1. Milling was performed for 20 h using a SPEX 8000 mixer (1080 rpm). The

as-milled Si powder consists of micrometric agglomerates (median size ~6 µm, S_{BET} ~12 m^2 g^{-1}) made of sub-micrometric particles more or less welded together [20]. The conductive additive was ultrathin platelets of graphite consisting in the as-received state of short stacks of graphene sheets (diameter ~15 µm, thickness ~5–10 nm, S_{BET} = 74 m^2 g^{-1}, GM15 grade from XGSciences). The binder was carboxymethyl cellulose (CMC) (DS = 0.9, Mw = 700 000, Sigma-Aldrich). Citric acid (CA) and KOH (Sigma-Aldrich) were used to prepare the pH3 buffer solution (0.17 M citric acid + 0.07 M KOH) as slurry medium.

2.2 Electrode preparation

For the standard electrode, a slurry was prepared by mixing 160 mg of silicon, 24 mg of GM15 conductive additive in 1 mL of CMC binder in pH3 buffer solution using a Fritsch Pulverisette 7 mixer at 500 rpm for 1 h with 3 silicon nitride balls (9.5 mm diameter). The pH3 buffering of the slurry promotes covalent bonding (esterification) between -OH groups present on the surface of Si particles and -COOH groups of CMC, which improves the mechanical and electrochemical stabilities of the electrode. [21,22] The slurry was tape casted by using a doctor blade onto a 25 µm thick copper current collector (PI-KEM, purity 99.9%, cold-rolled Cu foil) and dried 12 h at room temperature and then 2 h at 100°C under vacuum. Citric acid (CA) and KOH salts, which are not eliminated upon drying, contribute to the mass of the electrodes. The Si areal mass loading was typically 1.4 to 1.6 mg cm^{-2}. Matured electrode was obtained by storing the standard electrode under humid atmosphere (about 80% RH) for 3 days before final drying at 100°C and cell assembling. For the Cu-containing electrode, the slurry was prepared as for the standard electrode, except that the 1 mL of CMC binder in pH 3 buffer solution also contains a certain amount of $CuSO_4$ ($CuSO_4$,$5H_2O$, Alfa Aesar, purity 99.9%).

Reference samples were also prepared for the sake of complementary characterizations. For infrared (IR) spectroscopy and X-ray photoelectron spectroscopy (XPS) analyses, Si/CMC/CA/KOH/$CuSO_4$ samples were prepared in the same way as for their corresponding electrodes but without the carbon additive. After drying at 100°C under vacuum, a small amount of the film was scratched from the copper current collector. For XPS analysis, a Si/CMC sample referred as pH7 was prepared without using a CA/KOH buffer solution. Another sample analogous to the binder phase of a Cu-containing electrode was prepared with CMC/CA/KOH/$CuSO_4$ in the same proportion as for the Cu-0.05 electrode.

2.3 Characterization

Na, K and Cu contents in the matured electrodes were measured by inductively coupled plasma optical emission spectroscopy (ICP-OES, 5110 ICP-OES Instrument).

Diffuse reflectance infrared Fourier transform (DRIFT) spectroscopy characterizations were done with a vertex 70 Bruker spectrometer equipped with a Harrick HVC accessory, in the 400-4000 cm^{-1} range. No baseline correction was applied.

Solid state magic angle spinning nuclear magnetic resonance (MAS NMR) spectra were acquired on a 500 MHz Bruker Avance III using a 4mm MAS probe. For both ^{1}H-^{29}Si and ^{1}H-^{13}C Cross-Polarization (CP) spectra, the contact time was set to 2 ms. The recycle delay between scans was set to 2 s and the MAS frequency to 11 kHz and 10 kHz for ^{13}C and ^{29}Si acquisitions, respectively. TPPM15 ^{1}H decoupling scheme was used during all acquisitions with radiofrequency strength of 60 kHz. Spectra were referenced against TMS (tetramethylsilane).

XPS measurements were performed with a Kratos Axis Nova Instrument, using a monochromated Al K_α source (1486.6 eV) operating at 300 W. The instrument base pressure was 5×10^{-10} Torr. The sample area analyzed was about 700 µm × 300 µm. A pass energy (PE) of 80 eV, with an all over instrumental resolution of 0.9 eV measured on Fermi edge, was used to acquire wide range survey spectra. A PE of 40 eV was used to acquire narrow spectra of the C 1s, O 1s, Si 2p, Cu 2p and Na 1s levels with an all over instrumental resolution of 0.55 eV measured on Fermi edge. All data were acquired using charge compensation with low energy electrons gun in order to have homogenous surface potential. This is necessary to have accessible chemical information. XPS data were analyzed using the CasaXPS software (version 2.3.19) using Gaussian/Lorentzian (30% Lorentzian) line shapes and Shirley background correction. All spectra were calibrated with Hydrocarbon C1s photoemission set to 285.0 eV binding energy. In order to check for reproducibility, all XPS measurements are carried out in three independent areas of the samples.

All NMR, IR and XPS characterizations were done on samples dried at 100°C under vacuum.

2.4 Electrochemical measurement

Swagelok type half cells were assembled with the silicon electrodes (0.785 cm^2 disc) in a glovebox under argon atmosphere. A borosilicate glass-fiber (Whatman GF/D) was used as a separator and was soaked with an electrolytic solution of 1 M $LiPF_6$ in ethylene carbonate (EC) and dimethyl carbonate (DMC) (1:1) with 10 wt. % fluoroethylene carbonate (FEC) (Solvionic, purity 99.9%). A lithium foil (Aldrich, purity 99.9%) was used as the counter and reference electrode. The cycling tests were performed at room temperature in galvanostatic mode at full capacity over the potential window of 1-0.005 V versus Li^+/Li with a VMP multichannel electrochemical workstation (Bio-Logic). The current density was fixed at 96 mA per g of Si

(C/40) for the first cycle, then at 193 mA g^{-1} Si (C/20) for cycles 2 to 5 and then at 385 mA g^{-1} Si (C/10) for the following ones. The gravimetric capacities of the electrodes are given per mass of Si.

3. Results

Table 1 gives the as prepared standard and Cu-containing electrodes compositions. The composition of the matured electrode is expected to be identical to the standard one. However, its composition in Na, K and Cu was measured by ICP-OES (see below). The molar ratio of the amount of copper to the amount of carboxylate groups is also given in Table 1. This ratio is calculated as follows:

$$R_{Cu/COOH} = \frac{n_{Cu}}{3 \times n_{CA} + 0.9 \times n_{HCMC}}$$

where n_{CA} is the number of moles of citric acid, which has three carboxylates per molecule, and n_{HCMC} is the number of moles of CMC repetition (anhydroglucose) units, which has 0.9 carboxymethyl groups per unit.

ICP-OES measurements were done to quantify the elemental composition in K, Na and Cu of the electrode matured for various durations. Results are given in **Table 2**. K and Na are internal standard. They come from the citric acid/KOH buffer and the Na-CMC binder, while Cu was not part of the electrode formulation in this case. We assume that its presence is not due to the mechanical removing of the electrode from the current collector as we took care to not scratch the collector. Otherwise Cu would be heterogeneously distributed, in contradiction with the XPS analysis which confirm the homogeneity of the electrode. The most likely origin of the presence of copper in these electrode is the result of its atmospheric corrosion by the organic acids present in the electrode, respectively citric acid and the acidic form of carboxymethyl cellulose. [16,23] Indeed, traces of corrosion were previously observed at the surface of the collector. [16] We assume that the copper ions released during this atmospheric corrosion could have migrated into the humidified electrode during maturation. The amount of Cu in the electrode increases almost linearly with the duration of maturation to reach 1.67 wt.% of the total electrode mass after 7 days of maturation, which corresponds to $R_{Cu/COOH}$ equal to 0.18. One can notice that the amounts of K and Na stay constant, which attests of the good reproducibility of the composition of the electrode samples. Surprisingly, the un-matured electrode also contains traces of Cu. This might reflect the small corrosion of the current collector in contact with the acid electrode slurry during the casting and the drying steps.

Finally, by maturing the electrode for 2-3 days or deliberately adding about 2.5 wt.% of $CuSO_4$ ($R_{Cu/COOH} = 0.11$) in the electrode, one has the same electrode composition in the end, except for sulfate ions.

The electrochemical behavior (discharge capacity vs. cycle number) is shown in **Figure 1** for the three types of electrodes. It confirms the much better cyclability of the matured electrode compared to the standard case, as already shown in previous works. [15-17,19] The Cu-containing electrodes also display better cyclability than the standard electrode. The capacity retention is already significantly improved for the lower amount of $CuSO_4$ (1.30 wt%, $R_{Cu/COOH} = 0.054$) and reaches similar or slightly superior capacity retention than the matured electrode for 2.5 wt% of $CuSO_4$ ($R_{Cu/COOH} = 0.11$). For larger amounts of $CuSO_4$ (4.84 and 9.3 wt%, $R_{Cu/COOH} = 0.21$ and 0.43), there is no longer any performance improvement.

The discharge capacity retained after 100 cycles for the different electrodes is plotted against the molar ratio of the amount of copper to the amount of carboxylates in **Figure 2**. The trend is very clear. The retained capacity evolves considerably with the increase of $R_{Cu/COOH}$, up to a critical value of approximately 0.11. For a higher ratio, there is no longer any improvement in performance. The particular case of the matured electrode coincides with the trend curve of the electrodes in which copper has been deliberately added. It should be noted that in our previous work [16], we observed that 2 days were enough to get the maximum benefits from maturation. Leaving the electrode longer did not decrease or improve its cycling. This result is explained with this Figure 2 which shows that beyond a critical copper content there is no change in performance.

The ^{1}H-^{13}C CP-MAS NMR spectrum of a reference sample (in green) that does not contain citric acid but only Si particles and CMC is in agreement with the literature report for CMC [14] with resonances of C_1 (carboxylate/ic group) at 179 ppm, C_2 at 106 ppm, and substituted C_3 at 64 ppm, respectively (**Figure 3a**). The signals of other carbons from the ring and the chain are poorly resolved and span from 70 to 90 ppm. The spectrum for the standard electrode (in red) shows in addition the characteristic resonances for citric acid, namely the CH_2 group at 44 ppm (C_4), and the carboxylate/ic group at 173 ppm (C_5) is more intense than for the reference sample. The central carbon atom C_6 is expected at 75 ppm, thus overlaps with the main resonance of CMC. On the spectrum of the matured electrode (in blue), there is a huge loss of signal. The resonance of the citric acid (C_4) as well as those of the carboxylate/ic groups of citric acid and CMC (C_1 and C_5) are no longer visible. Only the signals of C atom of the CMC ring remain discernible. A first possible explanation for this loss of signal is an increase

of mobility of both CMC and citric acid after maturation which would impede the polarization transfer from ^{1}H to ^{13}C in the CP experiment. However, such an explanation is ruled out since no more signal was obtained by running a ^{1}H-^{13}C CP-MAS experiment at lower temperature (230K) for which residual mobility is too low to hinder CP transfer. Therefore, the most likely explanation for the loss of signal is the commitment of a fraction of the carboxylate groups belonging to both species in coordination bonds with copper ions throughout the whole electrode volume. Indeed, paramagnetic Cu(II) will ruin the CP polarization transfer by strongly decreasing the rotating frame spin lattice relaxation times ($T_{1\rho}$).

Additional information can be obtained from ^{29}Si NMR spectroscopy. The ^{1}H-^{29}Si CP-MAS spectra of the reference, standard and matured electrodes look similar (**Figure 3b**), all composed of three resonances. The ones at -80 ppm and -100 ppm originate from the bulk and the surface of the silicon particles, respectively [24]. The broad resonance at about -10 ppm suggests the formation of Si-C linkages (*e.g.* silane). The unexpected signal at -167 ppm in the spectrum of the standard electrode could be tentatively attributed to Si_5H_{12} molecules. [25] These silanes could be formed during the slurry mixing by high energy ball-milling through scission of the CMC chains and grafting to the silicon particles surface. In contrast with the ^{1}H-^{13}C CP-MAS spectra, the ^{1}H-^{29}Si CP-MAS signal of the electrode is still observable after maturation. Therefore, the complexation of copper by CMC and citric acid does not take place in the vicinity of the Si particle surfaces. Finally, the ^{1}H-^{29}Si CP-MAS signal spectrum of the matured electrode shows significant modification in the relative intensities of the 3 resonances as compared to the reference and standard electrodes. Since no loss of Si-C linkages (at -10 ppm) is expected during maturation, the relative increase in -80 and -110 ppm resonances intensities can be ascribed to better efficiency of the CP magnetization transfer. This improvement could proceed from water molecules and/or more CMC / citric acid –COOH groups interacting with the surface of the Si particles. In fact, the latter hypothesis is well supported by IR and XPS characterizations as shown below.

Diffused reflectance IR Fourier transform (DRIFT) spectra of the pristine silicon powder and of the electrodes, without however the carbon additive in their composition, are shown in **Figure 4a**. In the carbonyl region, the standard electrode shows an intense peak at ca. 1720-1730 cm^{-1}, which is attributed to the vibration of a C=O group engaged in R–C(=O)-O-Si ester bonds formed between the carboxylate groups of CMC and/or CA and the silanols at the silicon particles surface [26,27] in agreement with the concomitant decrease of the band located at ca. 1990 cm^{-1} and attributed to SiOH groups (see the reference Si material Figure 4a).

Nevertheless, the presence of purely organic R–C(=O)-O-R' ester formed by the reaction between CMC and CA is also possible. [28] There are also two less intense peaks centered at ca. 1610 cm^{-1} and 1405-1425 cm^{-1}, and corresponding to the anti-symmetric ($\nu_{asym}(CO_2^-)$ and symmetric vibrations ($\nu_{sym}(CO_2^-)$) of the carboxylate groups respectively. With maturation, the intensity of the peak at 1728 cm^{-1} decreases while that of the carboxylate centered at 1610 cm^{-1} increases. A very similar trend is observed upon the deliberate addition of $CuSO_4$: the band at 1720-1730 cm^{-1} decreases while the band at 1610 cm^{-1} increases (**Figure 4b**). These changes indicate that maturation caused the hydrolysis of the ester bonds, restoring carboxylate moieties. Knowing that carboxylate groups interact more strongly with copper(II) than alkaline ions, these groups are very likely involved in citrate-copper and CMC-copper coordination bonds. Asymmetric and symmetric carboxylates bands are known to be sensitive to the neighboring cations, and thus a good probe of the coordination. [29] Unfortunately, considering the copper to carboxylate ratio in play (here 0.05 to 0.43), both bands likely contain here not only contributions from copper(II) carboxylates bonds, but also sodium and potassium carboxylate bonds precluding any complete analysis.

Nevertheless, some changes are visible: first, upon increasing the amount of $CuSO_4$, whereas the position of the asymmetric band remains unchanged, a shift of the symmetric vibration band from ca. 1405 to 1425 cm^{-1} is observed (see insert on Figure 4b), leading to a value of $\Delta(\nu_{asym}(CO_2^-) - \nu_{sym}(CO_2^-))$ equal to 188 cm^{-1} for the copper rich samples (Cu-0.21, Cu-0.43) *versus* 206 cm^{-1} for the copper poor samples (Cu-0.05, Cu-0.11) and Na-CMC, testifying the occurrence of more copper(II) carboxylate bonds in copper rich samples. Second, even for a similar amount of copper, the spectra associated with the maturated electrode and the directly prepared Cu-containing electrode present slight differences, again on the symmetric vibration band. These changes, although, as mentioned above, difficult to fully decipher, are probably related to *(i)* a difference in the relative amount of sodium, potassium and copper carboxylate bonds, *(ii)* a difference in the relative amount of bound citrate and CMC, as well as *(iii)* different coordination modes of the copper-carboxylate pair. Whereas the direct introduction of copper sulfate in the electrode slurry likely leads to homogenous mixtures, and hence a final composition defined by the relative affinity constants of the constituents, the maturation procedure is likely more kinetically limited, and hence could lead ultimately to another coordination pattern

The C 1s-K 2p, Si 2p and Cu 2p XPS core peaks of standard silicon-based electrodes (prepared at pH7 and pH3, thus without CA/KOH in the first case), a matured silicon-based electrode (prepared at pH3) and an AC-CMC-Cu powder reference sample are shown in

Figures 5. The C 1s core peaks (figures 5a, d, g and j respectively) show the presence of four main components: the one at 285.0 eV (C1) is attributed to the hydrocarbon contribution (C-C/C-H), which is mainly contained in surface contamination, classically detected on the sample surfaces. The component located at 286.7 eV (C2) is assigned to alkyl **C**-O species, mainly contained in the CMC and CA compounds. The peak detected at 288.1 eV (C3) could be attributed to the carbon O-**C**=O contained in sodium or potassium carboxylate R**C**OONa or R**C**OOK [30]. The carbon appearing at 289.1 eV (C4) is assigned to a different environment of the carboxyl group, which could be either a carboxylic acid R**C**OOH [31], an ester (R-**C**(=O)-OR'), or a Si or Cu-carboxylate bond (R-**C**(=O)-O-Si- or R-**C**(=O)-O-Cu-)). Indeed, the C 1s XPS core peak of the CMC-AC-Cu reference compound (without silicon) (Figure 5j) shows also the presence of both environments, which is in agreement with our peak assignments. Note that the C4/ C3 ratio increases from pH7 to pH3, in line with the formation of (R-**C**(=O)-O-Si-) ester bonds in acidic pH as previously observed. [27,32] For the matured electrode, the C4/C3 ratio decreases as the consequence of the hydrolysis of the ester bonds, as already observed by the IR experiments. As the signal of R**C**OOH, R-**C**(=O)-O-Si- , R-**C**(=O)-OR' and R-**C**(=O)-O-Cu- overlap, no information regarding the amount of copper-carboxylate bonds can be extracted from this analysis.

The Si 2p core peaks (**Figures 5b, e** and h) are split in two components Si $2p_{3/2}$ and Si $2p_{1/2}$ due to the spin-orbit coupling effect. Each Si 2p (Si $2p_{3/2}$-Si $2p_{1/2}$) couple corresponding to one component is identified with a defined color. Three slightly asymmetric contributions are identified for the standard (at pH7 and pH3) and matured electrodes. The first one (Si1), with a Si $2p_{3/2}$ peak located at 98.7 eV, is assigned to the elemental silicon. The second one (Si2) (Si $2p_{3/2}$ at 102.1 eV) is attributed to the Si-based ester and **Si**O_x ($x<2$) type environments, and the third peak (Si3) (Si $2p_{3/2}$ at 103.1 eV) can be assigned to surface **Si**O_2 and **Si**OH contribution [33-35]. It is first worth noting that both elemental and oxidized silicon components relative to the electrode prepared at pH7 (figure 5b) present a higher FWHM (Full Width at Half Maximum) than the ones relative to the electrodes prepared at pH3 (figures 5e and h). The former electrode presents also a higher global oxidized Si/elemental Si ratio. This can be attributed to the presence of more intermediate surface species **Si**$_x$O$_y$ at pH7, which are eliminated at acidic pH. Note that the Si2/Si3 ratio increases from pH7 to pH3 (from 0.4 to 1.1), which is again in agreement with the formation of Si-based ester at acidic pH. This ratio decreases (from 1.1 to 0.3) after the electrode maturation, supporting again the partial hydrolysis of the Si-ester bonds.

The copper element is detected on the matured electrodes, and to a lesser extent in the standard ones (pH3 and pH7) (**Figures 5c**, **f** and **i** respectively). This is in agreement with the ICP results and corroborates our hypothesis of copper migration for the matured electrode. The Cu 2p core peaks are also split in two components due to the spin-orbit coupling phenomena (Cu $2p_{3/2}$ and Cu $2p_{1/2}$ with an area ratio of 2). It is worth to mention that the analysis of Cu-containing samples by XPS is challenging because of the copper reduction under the X-ray beam, impeding a quantitative analysis of the different oxidation states, especially in copper-poor samples. In order to be able to carry a comparative study, we fixed the measurement time constant for all the samples (30 min) and thus assume that the amount of copper reduced under the beam is the same for all the samples. Note that the metallic copper is characterized by a Cu $2p_{3/2}$ component appearing at 933.1 eV. However, the Cu(II) environment is generally recognized by a Cu $2p_{3/2}$ component at 935.0 eV and a first satellite peak at 940.9 eV [36]. If we consider the Cu 2p core peaks of the standard (pH3 and pH7), both contain a low amount of copper (0.2-0.3 at%), all in the reduced state. In line with the ICP measurement, this value reaches 0.7 at% for the maturated electrode, in which both reduced and oxidized copper are detected. Finally, the AC-CMC-Cu reference sample (figure 5k) contains a high proportion of copper (9.5 at%), with 0.4 at% the reduced state. All these analyses first suggest than in our experimental conditions, ca. 0.4 at% Cu is reduced under the beam, but also that copper is at least partially in the +II oxidation state in the maturated electrode.

XPS analyses were also conducted on the Si-electrodes prepared on a Cu-free substrate and to which were added different amounts of $CuSO_4$. The corresponding Si 2p XPS spectra are shown in **Figure 6**. The same silicon environments Si1, Si2 and Si3 are found as for the Si-electrodes prepared on a copper current collector (Figure 5). Nevertheless, we note a shift of the global Si spectra to higher binding energies with the addition of higher amounts of $CuSO_4$. We assume that this phenomenon rather originates from a more oxidant environment than from the formation of new species. Note that, unlike for the matured Si-electrode (Figure 5e), the Si2/Si3 ratio remains almost constant with the addition of $CuSO_4$. Indeed, these electrodes were not exposed to humid atmosphere contrarily to the matured electrode, and thus numerous ester bonds remain, in fair agreement with the IR results.

The C 1s XPS cores peaks corresponding to the Si-electrodes containing different amounts of $CuSO_4$ (Figure S1) show also four carbon environments (C1, C2, C3 and C4). Nevertheless, in this case, the evolution of the C4/C3 ratio seems to be more complex. Indeed, a different mechanism seems to be involved in the copper reactivity with the Si-based electrode

compared to the case of a matured electrode where the Si-based esters are partially hydrolyzed to form Cu-based ester and $RCOO^-$ carboxylates. This is again in agreement with IR analysis, which suggests different coordination patterns in the matured electrode than in the electrodes containing different amounts of $CuSO_4$ deliberately added. Given that the Si and Cu-based esters contributions are not dissociable (contribution C4), it is challenging to understand this different mechanism from the carbon peaks evolution. The Cu amount detected by XPS for this samples series of Si-based electrodes performed on a Cu-free substrate (Figure S2) is in agreement with the added amount of $CuSO_4$. Nevertheless, as previously detailed, it is quite challenging to consider the Cu oxidation number evolution given that this latter is reduced to Cu-metal under the X-ray beam.

Z. Yan and M.N. Obrovac [37] have found that the electrolyte is reduced in non-negligible quantity at low potential on metallic copper. This electrolyte reactivity is enhanced when this one contains vinylene carbonate (VC). Table 3 gives the coulombic efficiency (CE) and the irreversible capacity loss at the 1st and between the 2nd and the 100th cycles. In the case at hand, if the copper, which was deliberately added (or non- deliberately as a consequence of maturation) to the Si-based electrodes, was present in the metallic form, as nanoparticles for example, then the CE at the 1st cycle and for the following ones should decrease with the increase of the Cu content. The reverse trend is in fact observed (Table 3). The CE increases and the irreversible capacity loss decreases with an increase of the Cu content (**Figure 7**). This trend is in agreement with the XPS and IR analyses, which indicate that copper is rather present as cations involved in coordination bonds with the carboxylate moieties of the CA and CMC. In another work, Y. Gu et al., [38] added a Ni^{2+} salt to the alginate binder in silicon-based electrodes. They found that only ca. 10% on the Ni^{2+} was reduced to Ni^0 after cycling, suggesting that the coordination bond is stable in the 100 mV – 1V potential window. Moreover, they even observed an increase of the CE and a decrease of the amount of electrolyte degradation products for cations containing electrodes, suggesting a better stability of the SEI thanks to the addition of the cations. Our results are clearly in line with the work of Y. Gu et al.

Another information about the possible reduction of oxidized Cu species or the reduction of electrolyte on Cu is obtained by looking at differential capacity curves. Indeed, in their study, Yan and Obrovac observed on differential capacity curves one weak cathodic peak at 2.27 V and two strong cathodic peaks at 0.9 V and 1.3 V. [37] In the present study, the differential capacity of the first cycle does not clearly show extra peaks in Cu-containing electrode (Figure S3), which could be due to the fairly low amount of Cu in our electrodes compared to the study of Yan and Obrovac. However, the peak at 0.9-1.0V that corresponds to

the FEC reduction on these silicon-based electrodes, according to our previous work, [39] appears to be shifted to higher potential and its intensity is increased with higher Cu content. A study specifically dedicated to this phenomenon will have to be undertaken to explain this evolution.

4. Discussion

The initial atmospheric corrosion of copper induced by organic acids (formic, acetic, and propionic acid) was finely studied by Gil and Leygraf. [23] In their experimental conditions (exposure in 120 ppb (volume parts per billion) of carboxylic acid concentration in air (gas phase), 95% relative humidity, 20°C, and up to 4 days of exposure), they found that the corrosion products formed are mainly cuprous oxide or cuprite (Cu_2O), copper carboxylate, and water or hydroxyl groups. Two spatially separated main pathways, occurring at different sites of the copper surface, have been identified, as schematized in **Figure 8**.

The physically adsorbed water layer allows electrochemical reactions. The dominant ones are the oxidation of copper (anodic reaction: $Cu \rightarrow Cu^+ + e^-$) and reduction of oxygen (cathode reaction: $½\ O_2 + H^+ + 2\ e^- \rightarrow 2OH^-$). The first pathway for acid-induced atmospheric corrosion consists of proton-induced dissolution of Cu^+ ions, subsequent reaction of the Cu^+ ions with hydroxyl ions produced in the reduction of oxygen, and formation and precipitation of cuprite (Cu_2O). The second pathway consists of carboxylate-induced dissolution of Cu^+ ions, formation of dissolved Cu^+ or Cu^{2+} carboxylate species, that eventually precipitate as copper(II) carboxylate. The first pathway is initially very fast but levels off, grows more uniformly over the surface forming a layer up to about 15 nm thickness. The second pathway exhibits a more linear growth, with the formation of localized precipitates. The strength of the acid affects the corrosion process. A higher corrosion rate and domination of second pathway occurred with the stronger formic acid, because the stronger the acid, the higher the concentration of both protons and carboxylate ions for ligand exchange at the hydroxylated surface. For weaker acetic acid the first pathway dominated.

The conditions are different in our case, in particular because there is a mixture of organic acids (citric acid and the acid form of CMC) and because they are already present in the electrode in a significant amount. The exposure of the electrode to the humid atmosphere will cause the formation of a film of water on the surface of the electrode (in all its porosity) and on the surface of the copper collector. The acids present in the electrode and in the vicinity of the collector will be able to absorb this moisture or dissolve therein. It should therefore lead to the

corrosion of the copper collector, with the formation of Cu_2O- deposits and copper carboxylates. However, the presence of the electrode above the collector and the wet film on its surface can promote the diffusion of these copper carboxylates, and more particularly the low weight complexes formed with citric acid. As for the complexes formed between the CMC and the Cu^{2+} ions, their diffusion into the electrode from the current collector is less likely due to the multitude of attachment points of the long chains of CMC with the surface of the collector but also with the surface of the silicon or graphene particles. In the volume of the electrode, the absorption of water by the citric acid / CMC phase can lead to its swelling and to the formation of micro-gels in which the copper citrates (diffusing from the interface with the collector) could mix. After the maturation stage, the removal of the water by the drying stage would then lead to the formation of mixed copper complexes of citric acid and CMC. This would result in the formation of a very original three-dimensional network consisting of this mixture of CMC, citric acid, and Cu^{2+} ions. The nodes of this cross-linked network resulting from the formation of Cu^{2+} bridges or sequences of Cu^{2+} and citric acid linkers between the carboxylate lateral groups of the CMC chains.

These results are in line with previous studies focusing on alginate binders. It was indeed reported that the addition of cations (Ca^{2+}, Ba^{2+}, Zn^{2+}, Mn^{2+}, Al^{3+}) to sodium alginate gives rise to a net improvement of the cyclability of silicon and silicon-carbon based negative electrodes. [38,40-43] The cyclability improvement was related to the cross-linking of the alginate binder through the formation of carboxylate-cation coordination bonds, which significantly enhanced the mechanical strength of such electrode compared to the sodium alginate-based one. The examination of the influence of the cation size and charge showed that alginate-cation gels presenting the higher hardness and better retention of capacity upon cycling, were obtained from Al^{3+} and Ba^{2+} ions. [40] The amount of cations was also found to be critical: a ratio of 0.1 to 0.15 cation per alginate seemed optimal for achieving the better capacity retention. [39,41]

Matured electrodes show much superior mechanical strength, with three times higher resistance to peeling and seven times higher resistance to scratching than the standard electrode. [16] These superior mechanical properties may be ascribed to the physical cross-linking of the binder phase through the ligand (carboxylate)-Cu^{2+} coordination bonds. Recent reviews have highlighted a superiority trend of chemically cross-linked binders through covalent bonds, with respect to linear or ramified uncross-linked binders for silicon-based electrodes. [9-11] Cross-linked binders are stiffer than linear binder and therefore, during the delithiation of the active mass, they afford better elastic recovery of the electrode expansion that happened during

lithiation. However chemical cross-links are prone to irreversible and permanent rupture when stretched above a critical deformation point. Contrarily to covalent bonds, coordination bonds are labile. That means they are exchangeable and reversible, which afford self-healing properties to the resultant polymer-cation networks. [44] The recent reviews also emphasized another class of binders endowed with self-healing properties, which result from the presence of hydrogen bonding moieties in the binder. Hydrogen bonds, if reversible, are however weak, which minimizes the ability of such binders to give elastic recovery properties. Because coordination bonds are stronger than hydrogen bonds but still reversible, it appears that they might be the more suitable type of bond to rely upon for building a tough and resilient silicon-based electrode.

Physical cross-linking of the CMC/CA with (carboxylate)-Cu^{2+} coordination bonds can also be achieved by deliberately adding Cu(II) salt in the electrode slurry, allowing for similar level of electrochemical performance enhancement. However, both IR and XPS spectroscopies suggest that different coordination patterns and Si-CMC/CA bonding and thus different types of binding networks are formed in such electrode compared to the matured one. In particular, the amount of Si-CMC/CA ester bonds appear significantly different in both electrodes, the maturation causing the hydrolysis of numerous of these bonds. But these IR and XPS analyses relate to the as-prepared electrodes, just before cell assembling; the evolution of these microstructures upon cycling is largely possible. In particular, the reminiscence of the Si-CMC/CA ester bond upon lithium (de)alloying has never been proved. The similar electrochemical performance of the matured and $CuSO_4$–containing electrodes may suggest that the key parameter controlling the mechanical stability of the electrodes is the presence of Cu(II) ions distributed in the binder phase allowing for self-healing mechanical properties.

Finally, the beneficial influence of the addition of Cu^{2+} cations on the CE could be explained as follow. It was shown that binders such as alginate or CA/CMC behave as artificial SEI. [39,45-47] This is because they can form a thin electronically insulating and lithium conducting coating at the surface of the silicon particles. However, this binder layer may be disrupted during cycling as a consequence of the silicon particles volume variations. As described into more details in the Discussion section, the addition of cations to these binders improves their mechanical properties, which could be at the origin of better mechanical stability of the pre-formed artificial SEI and thus improved CE.

Conclusion

The superior mechanical strength of the matured electrode is due for a large part to the migration of Cu^{2+} ions from the current collector across the electrode thickness. These cations coordinate with the carboxylate groups of the carboxymethylcellulose binder and of citric acid to form a physically cross-linked network provided with both elastic and self-healing properties. As a result of this superior mechanical strength, the cyclability of matured electrode is largely enhanced with respect to un-matured one.

The same level of performance can however be achieved for a non-matured electrode by deliberately adding these Cu^{2+} ions in the electrode slurry, even if different coordination pattern is formed. In both cases, the maximum level of performance improvement is reached for a copper content of about 1 wt% that corresponds to a molar ratio of copper to carboxylates equal to about 0.11.

The convenience of the second approach, together with the myriad of possibilities associated with the selection of cations of various size and charge, polymers, and/or smaller organic molecules carrying various types and numbers of organic ligands, is offering a very attractive and also vertiginous avenue to explore for designing a novel class of binders for lithium-ion battery silicon-based electrodes, [48] and more generally for negative and positive composite electrodes for various types of batteries and also super-capacitors.

Acknowledgements

The authors thank the Natural Sciences and Engineering Research Council (NSERC) of Canada and the Centre National de la Recherche Scientifique (CNRS) of France for supporting this work. D. M. is grateful to the University of Nantes for invited stay.

References

[1] M.N. Obrovac, V.L. Chevrier, Alloy negative electrodes for Li-ion batteries. Chem. Rev. 114 (2014) 11444–11502.

[2] U. Kasavajjula, C. Wang, A. J. Appleby, Nano- and bulk-silicon-based insertion anodes for lithium-ion secondary cells. J. Power Sources 163 (2007) 1003–1039

[3] J. R. Szczech, S. Jin, Nanostructured silicon for high capacity lithium battery anodes. Energy Environ. Sci. 4 (2011) 56.

[4] H. Wu, Y. Cui, Designing nanostructured Si anodes for high energy lithium ion batteries. Nano Today 7 (2012) 414-429.
[5] X. Su, Q. Wu, J. Li, X. Xiao, A. Lott, W. Lu, B. W. Sheldon, J. Wu, Silicon-Based Nanomaterials for Lithium-Ion Batteries: a review. Adv. Energy Mater. 4 (2014) 1300882.
[6] J.W. Choi, D. Aurbach, Nature reviews materials 1 (2016) 1-16.
[7] M.N. Obrovac, Si-alloy negative electrodes for Li-ion batteries. Current Opinion in Electrochemistry 9 (2018) 8–17.
[8] D. Mazouzi, Z. Karkar, C. Reale Hernandez, P. Jimenez Manero, D. Guyomard, L. Roué, B. Lestriez, Critical roles of binders and formulation at multiscales of silicon-based composite electrodes, J. Power Sources 280 (2015) 533-549.
[9] J-T. Li, Z-Y. Wu, Y-Q. Lu, Y. Zhou, Q-S. Huang, L. Huang, S-G. Sun, Water Soluble Binder, an Electrochemical Performance Booster for Electrode Materials with High Energy Density Adv. Energy Mater. 7 (2017) 1701185.
[10] H. Chen, M. Ling, L. Hencz, H. Y. Ling, G. Li, Z. Lin, G. Liu, S. Zhang, Exploring Chemical, Mechanical, and Electrical Functionalities of Binders for Advanced Energy-Storage Devices, Chem. Rev. 118 (2018) 8936−8982.
[11] T. Kwon, J.W. Choi, A. Coskun, The Emerging Era of Supramolecular Polymeric Binders in Silicon Anodes. Chem. Soc. Rev. 47 (2018) 2145–2164.
[12] D. Bresser, D. Buchholz, A. Moretti, A. Varzi, S. Passerini, Alternative binders for sustainable electrochemical energy storage – the transition to aqueous electrode processing and bio-derived polymers, Energy Environ. Sci. 11 (2018) 3096.
[13] N. Yabuuchi, K. Shimomura, Y. Shimbe, T. Ozeki, J.-Y. Son, H. Oji, Y. Katayama, T. Miura, S. Komaba, Adv. Energy Mater. 1 (2011) 759.
[14] J. S. Bridel, T. Azaïs, M. Morcrette, J. M. Tarascon, D. Larcher, Chem. Mater. 22 (2010) 1229–1241.
[15] C. Reale Hernandez, Z. Karkar, D. Guyomard, B. Lestriez, L. Roué, A film maturation process for improving the cycle life of Si-based anodes for Li-ion batteries. Electrochem. Comm. 61 (2015) 102-105.
[16] C. Reale Hernandez, A. Etiemble, D. Mazouzi, Z. Karkar, E. Maire, D. Guyomard, B. Lestriez, L. Roué, A facile and very effective method to enhance the mechanical strength and the cyclability of Si-based electrodes for Li-ion batteries, Adv. Energy Mater. 8 (2018) 1701787.

[17] V. Vanpeene, J. Villanova, A. King, B. Lestriez, E. Maire, L. Roué, Dynamics of the morphological degradation of Si-based anodes for Li-ion batteries characterized by in-situ X-ray tomography, submitted

[18] Z. Du, R. A. Dunlap, M. N. Obrovac, High Energy Density Calendered Si Alloy/Graphite Anodes. J. Electrochem. Soc. 161 (2014) A1698-A1705.

[19] Z. Karkar, T. Jaouhari, A. Tranchot, D. Mazouzi, D. Guyomard, B. Lestriez, L. Roué, How silicon electrodes can be calendered without altering their mechanical strength and cycle life, J. Power Sources 371 (2017) 136-147.

[20] M. Gauthier, D. Mazouzi, D. Reyter, B. Lestriez, P. Moreau, D. Guyomard, L. Roué, A low-cost and high performance ball-milled Si-based negative electrode for high-energy Li-ion batteries, Energy Environ. Sci. 6 (2013) 2145-2155.

[21] D. Mazouzi, B. Lestriez, L. Roué, D. Guyomard, Silicon composite electrode with high capacity and long cycle life, Electrochem. Solid-State Lett. 12 (2009) A215-A218.

[22] A. Tranchot, H. Idrissi, P. X. Thivel, L. Roué, Impact of the slurry pH on the expansion/contraction behavior of silicon/carbon/carboxymethylcellulose electrodes for Li-ion batteries, J. Electrochem. Soc. 163 (2016) A1020-A1026.

[23] H. Gil, C. Leygraf, Initial Atmospheric Corrosion of Copper Induced by Carboxylic Acids J. Electrochem. Soc. 154 (2007) C611.

[24] T. Pietraβ, A. Bifone, R.D. Roth, V.-P. Koch, A.P. Alivisatos, A. Pines, 29Si High Resolution Solid State Nuclear Magnetic Resonance Spectroscopy of Porous Silicon, J. Non-Crystalline Solids 202 (1996) 68–76.

[25] J. Hahn, 29 Si-NMR-spektroskopische Untersuchungen von geradkettigen und verzweigten Silanen. Z. Naturforsch 35b (1980) 282-296.

[26] N.S. Hochgatterer, M.R. Schweiger, S. Koller, P.R. Raimann, T. Wöhrle, C. Wurm, M. Winter, Silicon/Graphite Composite Electrodes for High-Capacity Anodes: Influence of Binder Chemistry on Cycling Stability, J. Electrochem. Solid State Lett. 11 (2008) A76.

[27] N. Delpuech, D. Mazouzi, N. Dupre, P. Moreau, M. Cerbelaud, J-S. Bridel, J-C. Badot, E. De Vito, D. Guyomard, B. Lestriez, B. Humbert. Critical Role of Si Nanoparticles Surface on Lithium Cell Electrochemical Performance Analyzed by FTIR, Raman, EELS, XPS, NMR and BDS Spectroscopies, J. Phys. Chem. C 118 (2014) 17318-17331.

[28] B. Koo, H. Kim, Y. Cho, K. Lee, N.-S. Choi, J. A. Cho, Highly Cross-linked Polymeric Binder for High-performance Silicon Negative Electrodes in Lithium Ion Batteries. Angew. Chem., Int. Ed. 51 (2012) 8762–8767

[29] X. Liu, B. Lin, Z. Zhang, H. Lei, Y. Li, Copper(II) carboxymethylcellulose (CMC-CuII) as an efficient catalyst for aldehyde–alkyne–amine coupling under solvent-free conditions, RSC Adv. 6 (2016) 94399-94407.

[30] G. Zou, Q. Zhang, C. Fernandez, G. Huang, J. Huang, Q. Peng, Heterogeneous Ti3SiC2@C-Containing Na2Ti7O15 Architecture for High-Performance Sodium Storage at Elevated Temperatures, ACS Nano 11 (2017) 12219−12229

[31] P. Louette, F. Bodino, J-J. Pireaux, Poly(acrylic acid) (PAA) XPS Reference Core Level and Energy Loss Spectra, Surface Science Spectra 12 (2005) 22-26.

[32] D. Mazouzi, B. Lestriez, L. Roué, D. Guyomard, Silicon Composite Electrode with High Capacity and Long Cycle Life, Electrochem. Solid-State Lett. 12 (2009) A215-A218.

[33] M. Sivakumar, K. Venkatakrishnan, B. Tan, Characterization of MHz pulse repetition rate femtosecond laser-irradiated gold-coated silicon surfaces, Nanoscale Research Letters 6 (2011) 78.

[34] I. Lisovskyy, M. Voitovych, A. Sarikov, V.G. Litovchenko, A. B. Romanyuk, V. Melnyk, I. M. Khatsevich, P. Shepeliavyi, V. Lashkarev, Transformation of the structure of silicon oxide during the formation of Si nanoinclusions under thermal annealings, Ukrainian Journal of Physics 54 (2009) 383-390.

[35] N. Liu, X. Huang, J. J. Dubowski, Selective area in situ conversion of Si (0 0 1) hydrophobic to hydrophilic surface by excimer laser irradiation in hydrogen peroxide, J. Physics D: Applied Physics 47 (2014) 385106.

[36] M. C. Biesinger, L. W. M. Lau, A. R. Gerson, R. St. C. Smart, Resolving surface chemical states in XPS analysis of first row transition metals, oxides and hydroxides: Sc, Ti, V, Cu and Zn, Applied Surface Science 257 (2011) 887-898.

[37] Z. Yan and M.N. Obrovac, Selecting inactive materials with low electrolyte reactivity for lithium-ion Cells, J. Power Sources 397 (2018) 374–381.

[38] Y. Gu, S. Yang, G. Zhu, Y. Yuan, Q. Qu, Y. Wang, H. Zheng, The effects of cross-linking cations on the electrochemical behavior of silicon anodes with alginate binder, Electrochimica Acta 269 (2018) 405-414.

[39] Z. Karkar, D. Guyomard, B. Lestriez, L. Roué, "A comparative study of polyacrylic acid (PAA) and carboxymethyl cellulose (CMC) binders for Si-based electrodes", Electrochimica Acta, 2017, 258, 453-466.

[40] J. Yoon, D.X. Oh, C. Jo, J. Lee, D.S. Hwang, Improvement of Desolvation and Resilience of Alginate Binders for Si-Based Anodes in a Lithium Ion Battery by Calcium-Mediated Cross-Linking. Phys. Chem. Chem. Phys. 16 (2014) 25628–25635.

[41] J. Liu, Q. Zhang, Z.-Y. Wu, J.-H. Wu, J.-T. Li, L. Huang, S.-G. Sun, A High-Performance Alginate Hydrogel Binder for the Si/C Anode of a Li-Ion Battery. Chem. Commun. 50 (2014) 6386–6389.

[42] L. Zhang, L. Zhang, L. Chai, P. Xue, W. Hao, H. Zheng, A Coordinatively Cross-Linked Polymeric Network as a Functional Binder for High-Performance Silicon Submicro-Particle Anodes in Lithium-Ion Batteries. J. Mater. Chem. A 2 (2014) 19036–19045.

[43] Z.-Y.Wu, L. Deng, J.-T. Li, Q.-S. Huang, Y.-Q. Lu, J. Liu, T. Zhang, L. Huang, S.-G. Sun, Multiple Hydrogel Alginate Binders for Si Anodes of Lithium-Ion Battery. Electrochimica Acta 245 (2017) 371–378.

[44] J.-C. Lai, L. Li, D.-P. Wang, M.-H. Zhang, S.-R. Mo, X. Wang, K.-Y. Zeng, C.-H. Li, Q. Jiang, X.-Z. You, A Rigid and Healable Polymer Cross-Linked by Weak but Abundant Zn(II)-Carboxylate Interactions. Nature Communications 9 (2018) 2725.

[45] S. Komaba, N. Yabuuchi, T. Ozeki, K. Okushi, H. Yui, K. Konno, Y. Katayama, T. Miura, Functional binders for reversible lithium intercalation into graphite in propylene carbonate and ionic liquid media, J. Power Sources 195 (2010) 6069.

[46] F. Jeschull, M.J. Lacey, D. Brandell, Functional binders as graphite exfoliation suppressants in aggressive electrolytes for lithium-ion batteries, Electrochim. Acta 175 (2015) 141.

[47] C.C. Nguyen, T. Yoon, D.M. Seo, P. Guduru, B.L. Lucht, Systematic investigation of binders for silicon anodes: interactions of binder with silicon particles and electrolytes and effects of binders on solid electrolyte interphase formation, ACS Appl. Mater. Interfaces 8 (2016) 12211.

[48] T. Devic, B. Lestriez, L. Roué, Silicon Electrodes for Li-Ion Batteries. Addressing the Challenges through Coordination Chemistry, ACS Energy Letters, 4 (2019) 550–557.

Figure captions

Figure 1. *Comparison of the electrochemical performance between standard, matured, and $CuSO_4$-added electrodes cycled at full capacity.*

Figure 2. *The discharge capacity retained after 100 cycles vs. the molar ratio of the amount of copper to the amount of carboxylates for the different electrodes: standard, matured, and those prepared by addition of $CuSO_4$ in their slurry formulation.*

Figure 3a. *^{1}H-^{13}C CP-MAS NMR spectra on standard (red, b) and matured (blue, a) electrodes (without carbon in their composition) scrapped of the copper collector. The spectrum of an electrode prepared without citric acid is also shown as reference (green, c).*

Figure 3b. *^{1}H-^{29}Si CP-MAS NMR spectra on standard (red, b) and matured (blue, a) electrodes (without carbon in their compositions) scrapped of the copper collector. The spectrum of an electrode prepared without citric acid is also shown as a reference (green, c).*

Figure 4. *DRIFT spectra of (a) the as-milled silicon powder, the standard and the matured electrodes (without carbon additive in their composition) removed from the copper collector; (b) of electrodes prepared with various amounts of $CuSO_4$ (also without carbon additive in their composition). Insert: zoom of the 1800-1200 cm^{-1} region.*

Figure 5. *C 1s-K 2p, Si 2p and Cu 2p XPS core peaks of a silicon electrode (at pH=7) ((a), (b), and (c) respectively), the standard Si-electrode (pH=3) ((d), (e) and (f) respectively, the matured electrodes ((g), (h) and (i) respectively) and an AC-CMC-Cu mixture powder ((j) and (k) respectively).*

Figure 6. *Si 2p XPS core peaks of a silicon electrode deposited on a Cu-free substrate and containing different amounts of $CuSO_4$ ([Cu]/[COOH] ratio =0 (a), 0.054 (b), 0.107 (c), 0.214 (d) and 0.429 (e).*

Figure 7. *The 1^{st} cycle irreversible capacity loss vs. the copper content in the different electrodes.*

Figure 8. *Schematic description of possible pathways for acid-induced atmospheric corrosion of copper. Reprinted from Reference [23], Copyright 2007, with permission from The Electrochemical Society.*

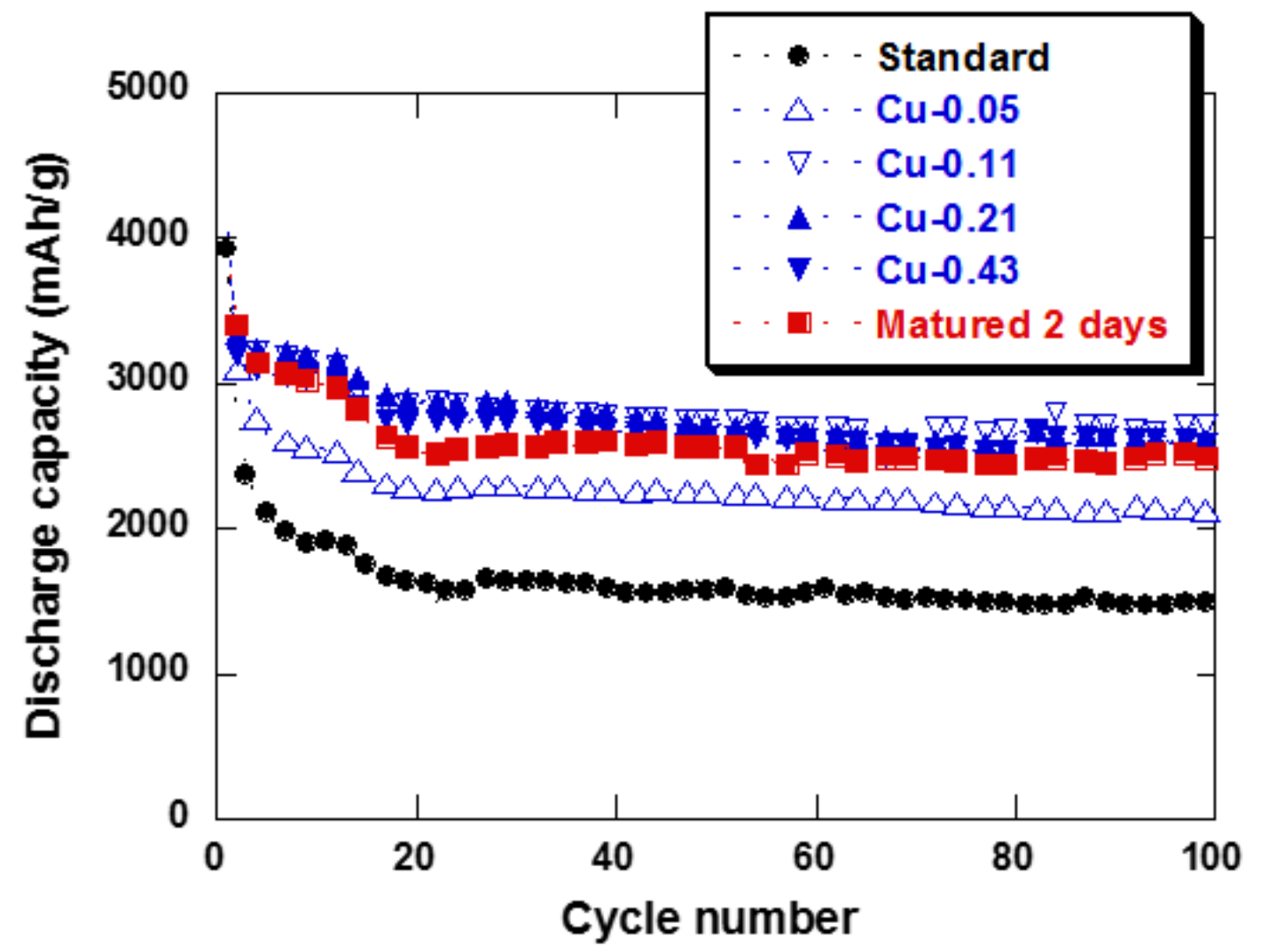
Standard
Cu-0.05
Cu-0.11
Cu-0.21
Cu-0.43
Matured 2 days
Discharge capacity (mAh/g)
Cycle number
0
1000
2000
3000
4000
5000
0
20
40
60
80
100

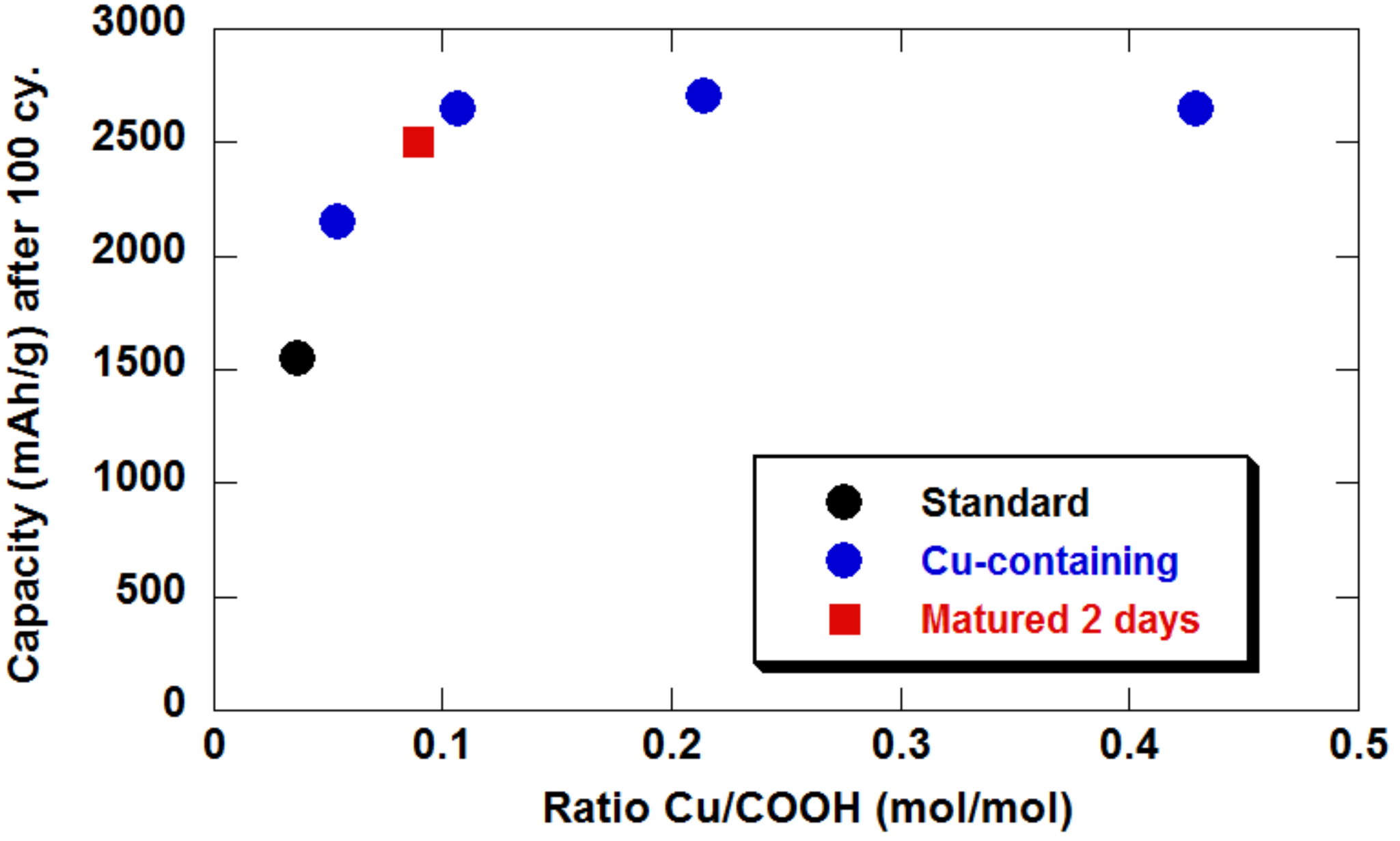
3000
2500
2000
1500
1000
500
0
Capacity (mAh/g) after 100 cy.
0
0.1
0.2
0.3
0.4
0.5
Ratio Cu/COOH (mol/mol)
Standard
Cu-containing
Matured 2 days

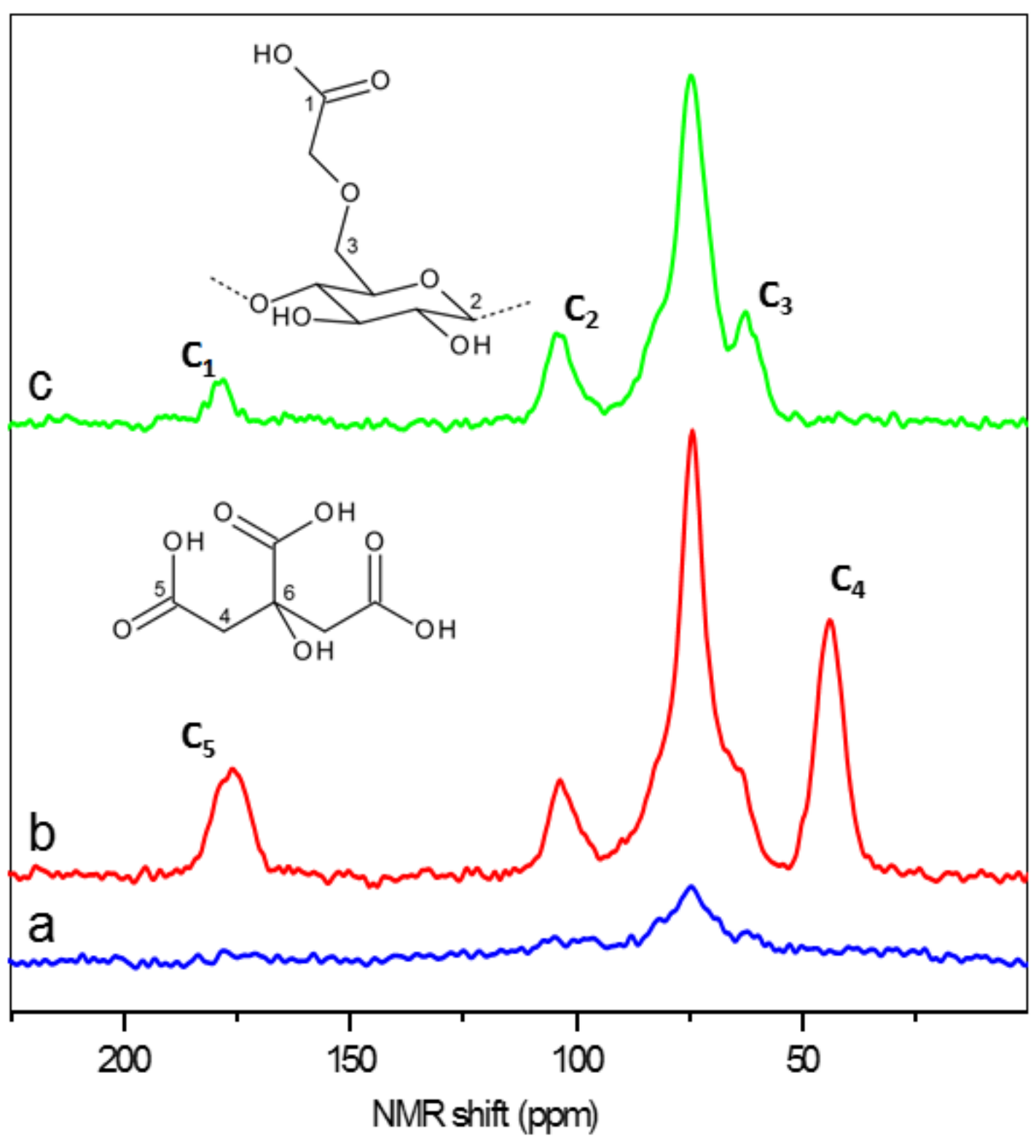
HO
O
1
O
3
O
HO
O
2
OH
C1
C2
C3
c
O
OH
OH
O
5
6
4
O
OH
OH
C4
C5
b
a
200
150
100
50
NMR shift (ppm)

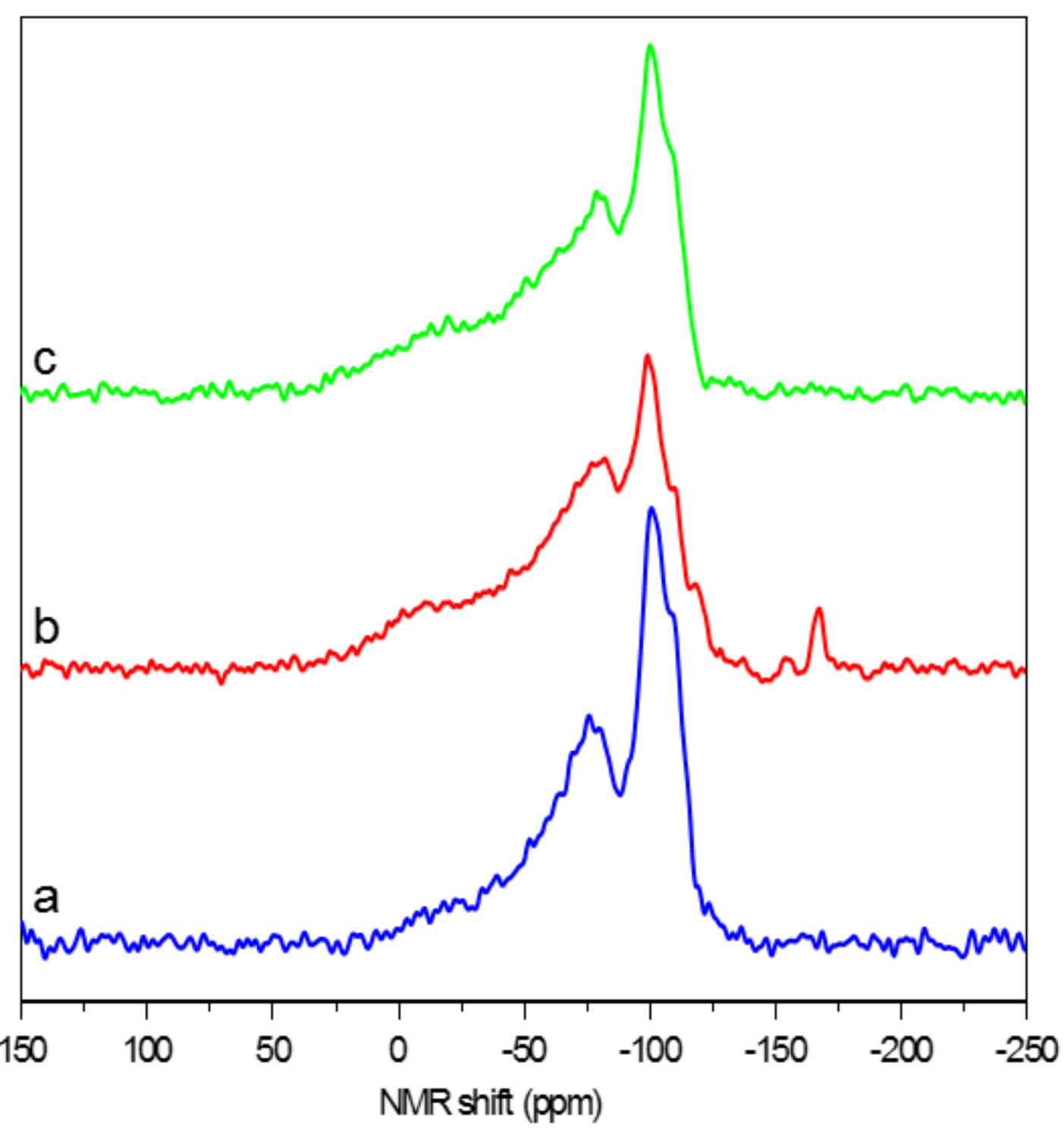
c
b
a
150
100
50
0
-50
-100
-150
-200
-250
NMR shift (ppm)

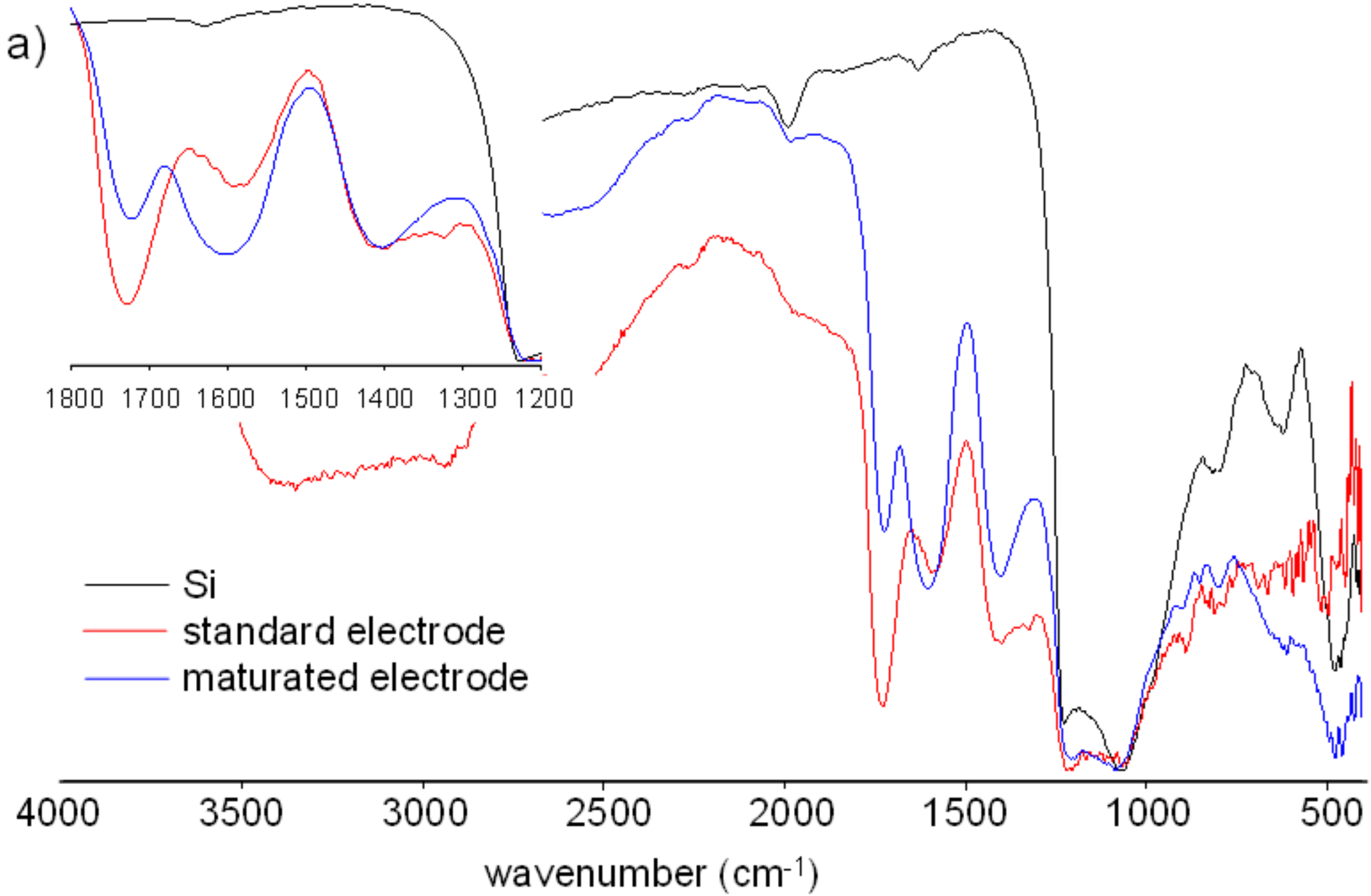
a)
1800 1700 1600 1500 1400 1300 1200
Si
standard electrode
maturated electrode
4000 3500 3000 2500 2000 1500 1000 500
wavenumber (cm-1)

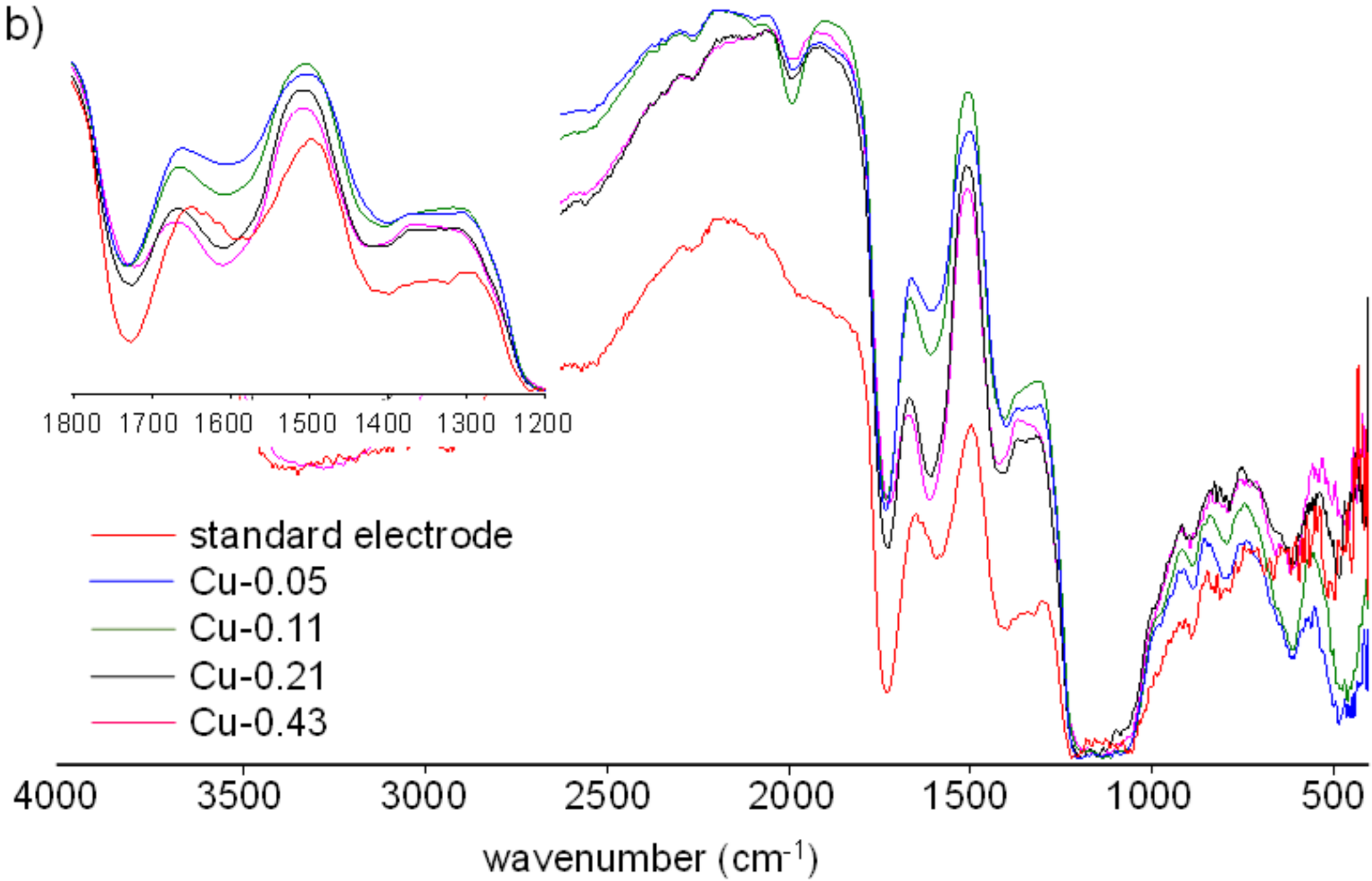
b)
1800 1700 1600 1500 1400 1300 1200
standard electrode
Cu-0.05
Cu-0.11
Cu-0.21
Cu-0.43
4000 3500 3000 2500 2000 1500 1000 500
wavenumber (cm-1)

C 1s

Si 2p

Cu 2p

Si-electrode (PH=7)

Standard Si-electrode (PH=3)

Matured Si-electrode (PH=3)

AC-CMC-Cu

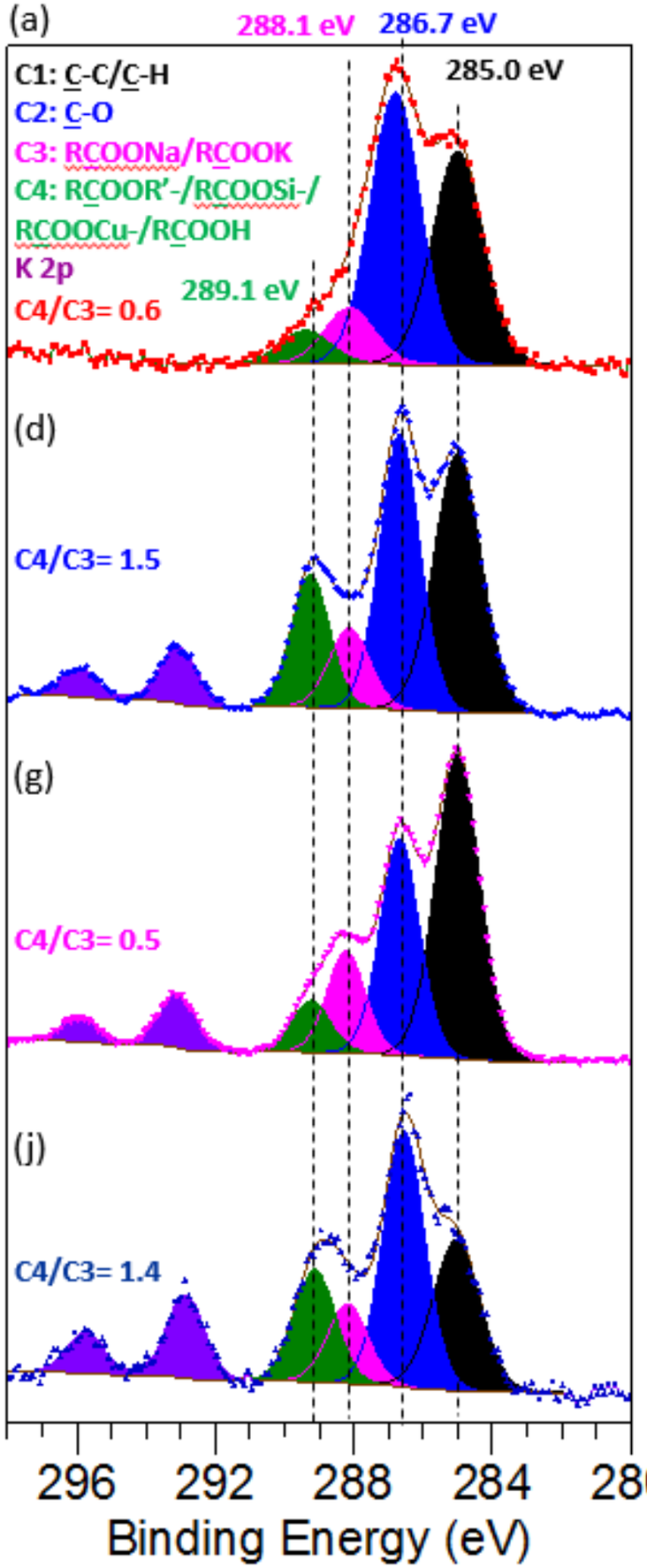

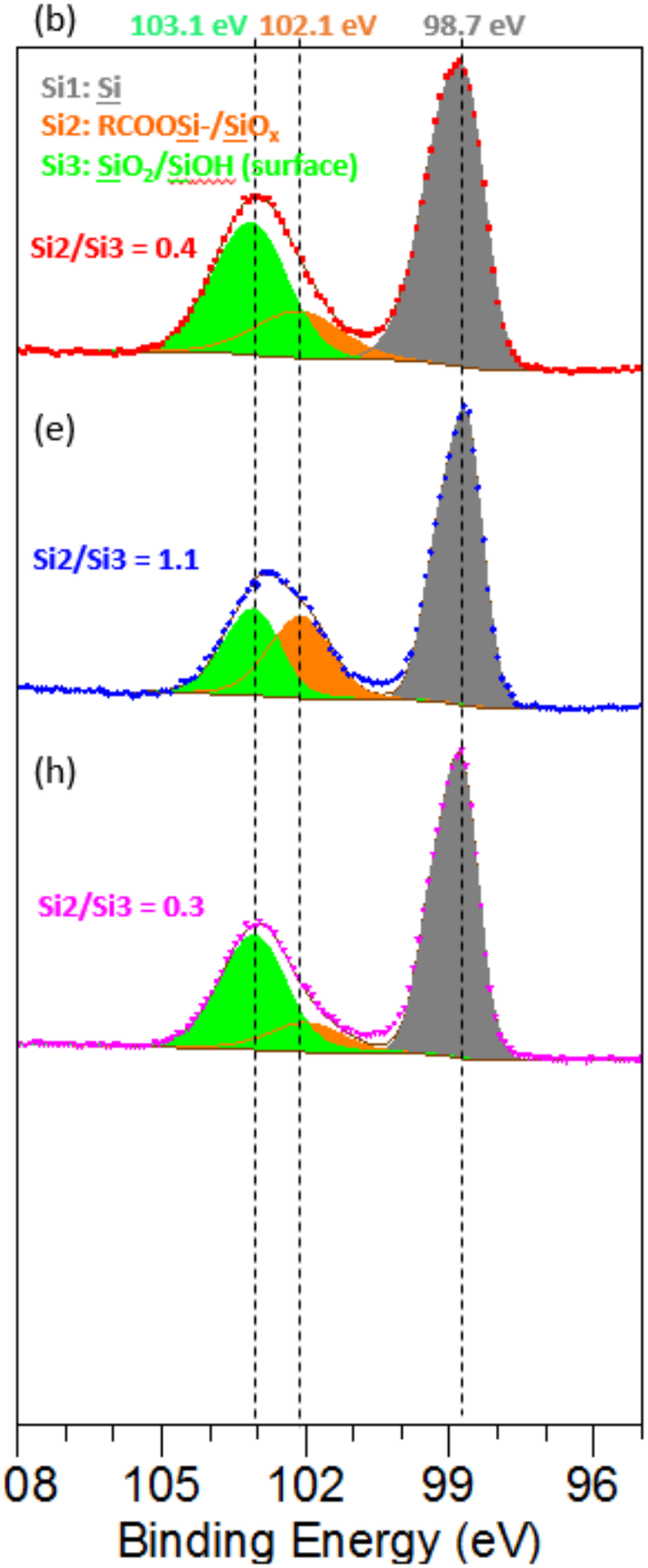

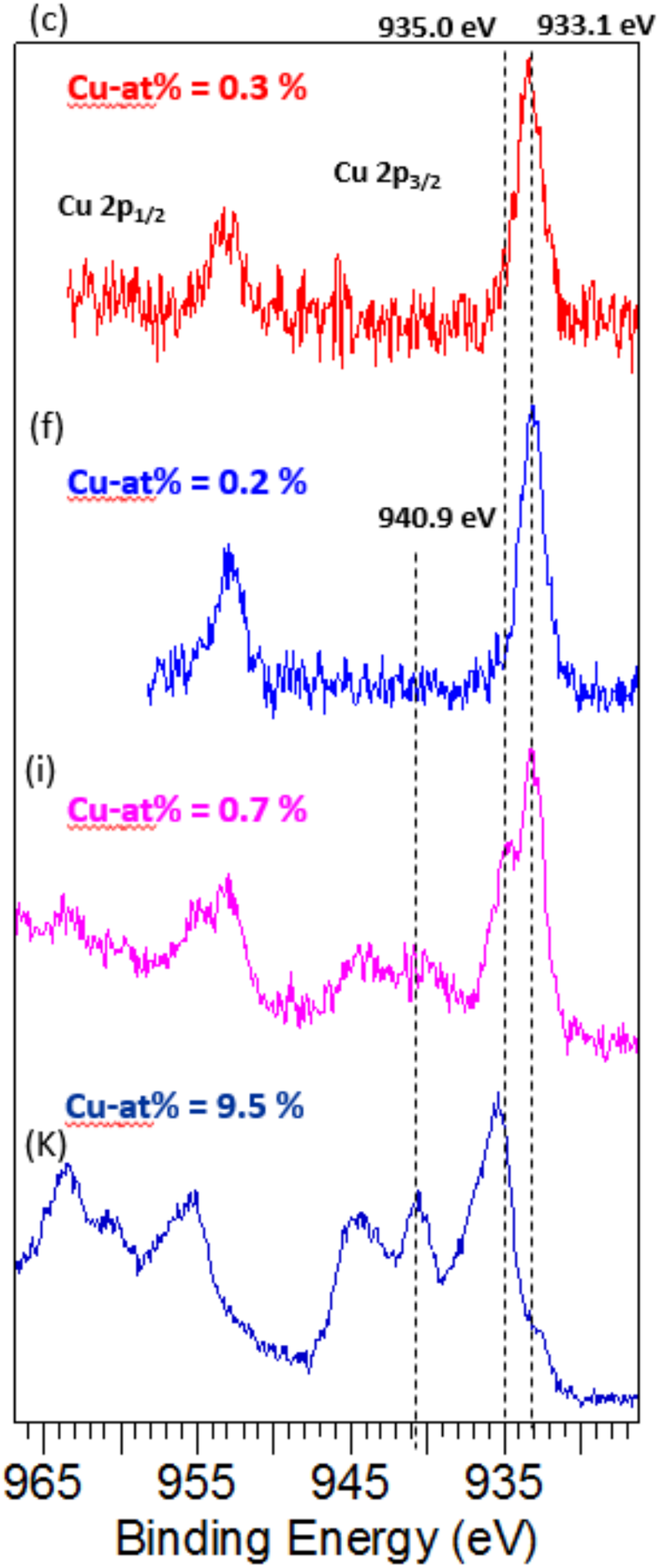

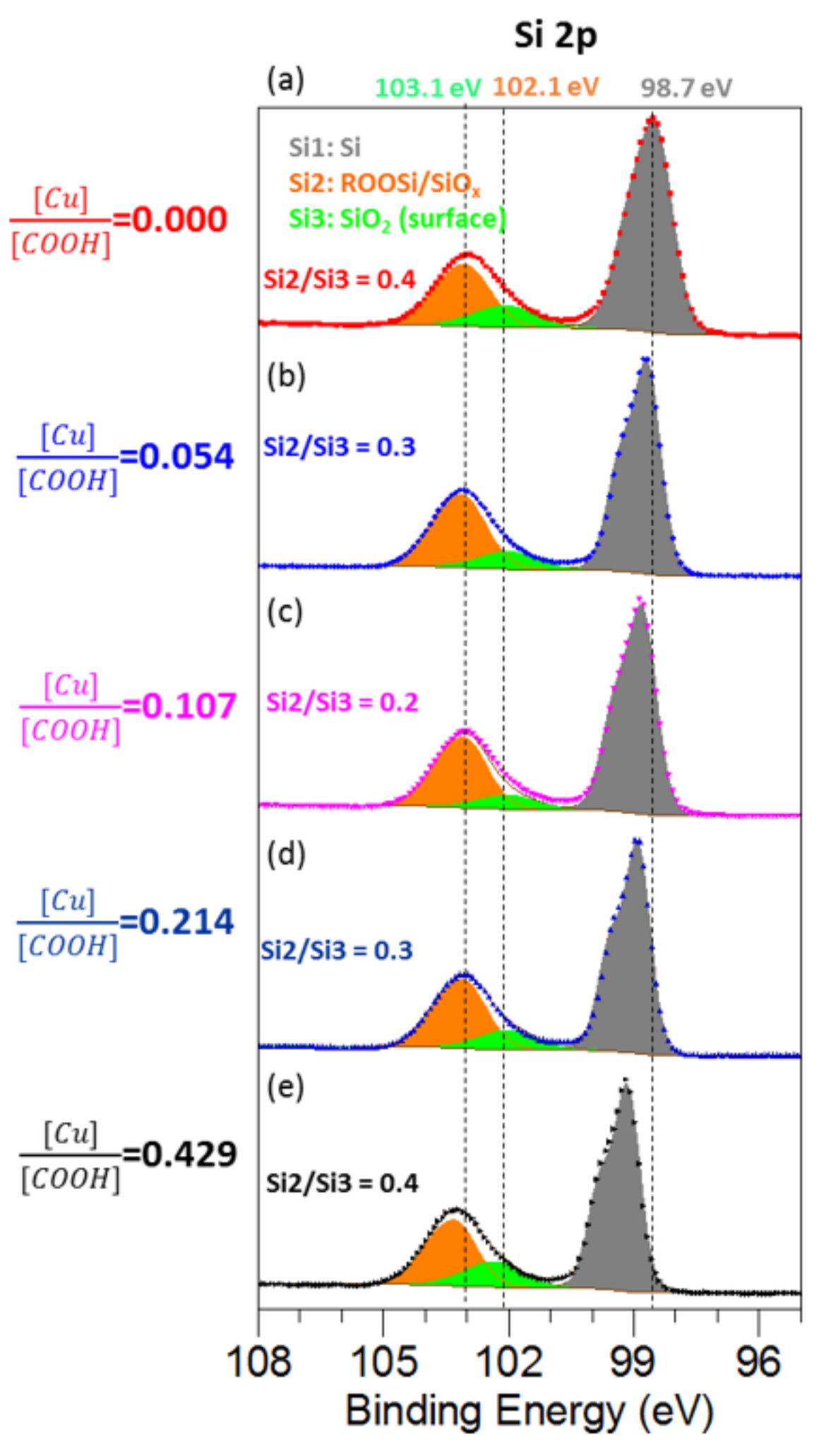
Si 2p
(a)
103.1 eV
102.1 eV
98.7 eV
Si1: Si
Si2: ROOSi/SiOx
Si3: SiO2 (surface)
Si2/Si3 = 0.4
(b)
Si2/Si3 = 0.3
(c)
Si2/Si3 = 0.2
(d)
Si2/Si3 = 0.3
(e)
Si2/Si3 = 0.4
[Cu]/[COOH]=0.000
[Cu]/[COOH]=0.054
[Cu]/[COOH]=0.107
[Cu]/[COOH]=0.214
[Cu]/[COOH]=0.429
108
105
102
99
96
Binding Energy (eV)

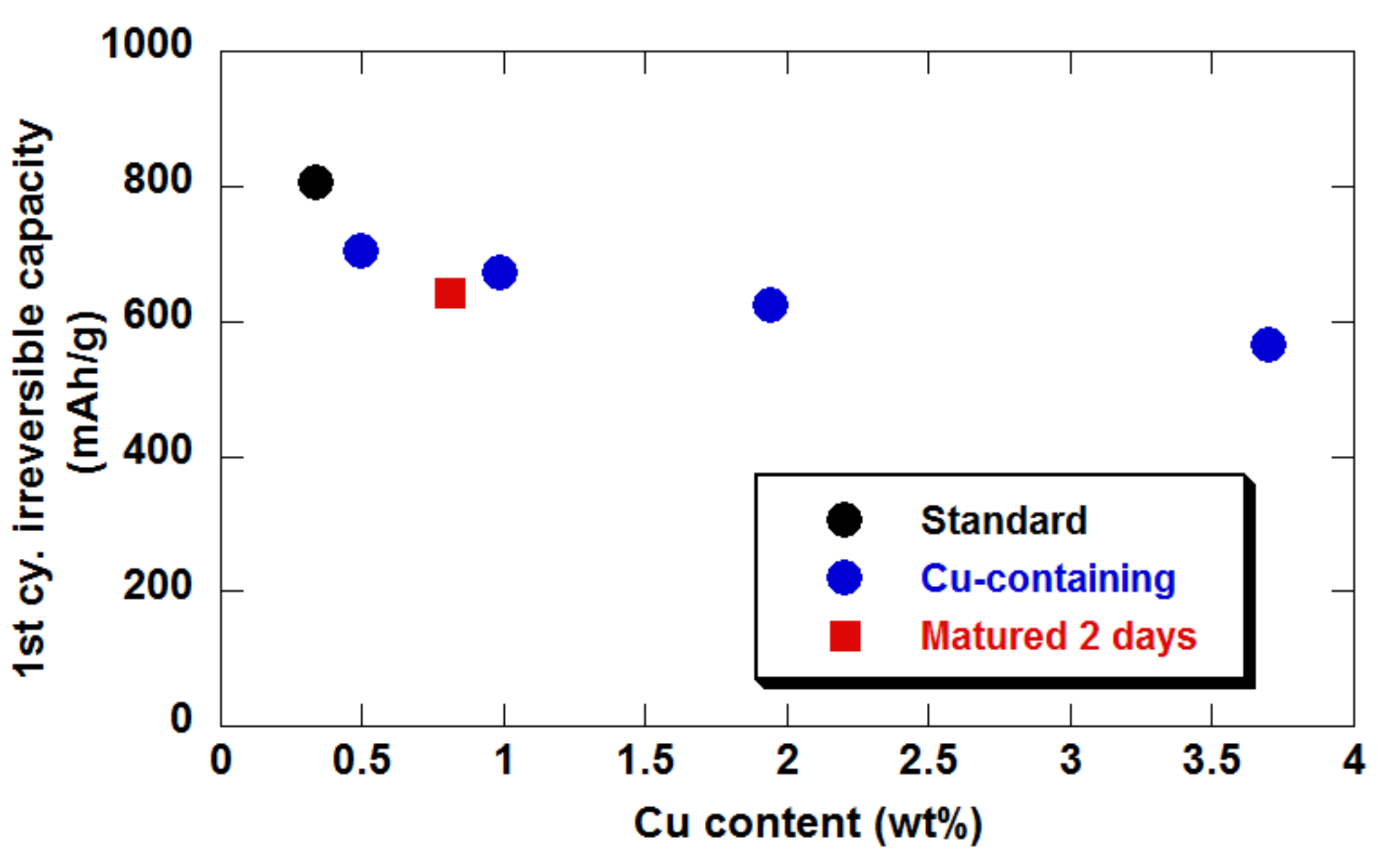
1000
800
600
400
200
0
1st cy. irreversible capacity (mAh/g)
0
0.5
1
1.5
2
2.5
3
3.5
4
Cu content (wt%)
Standard
Cu-containing
Matured 2 days

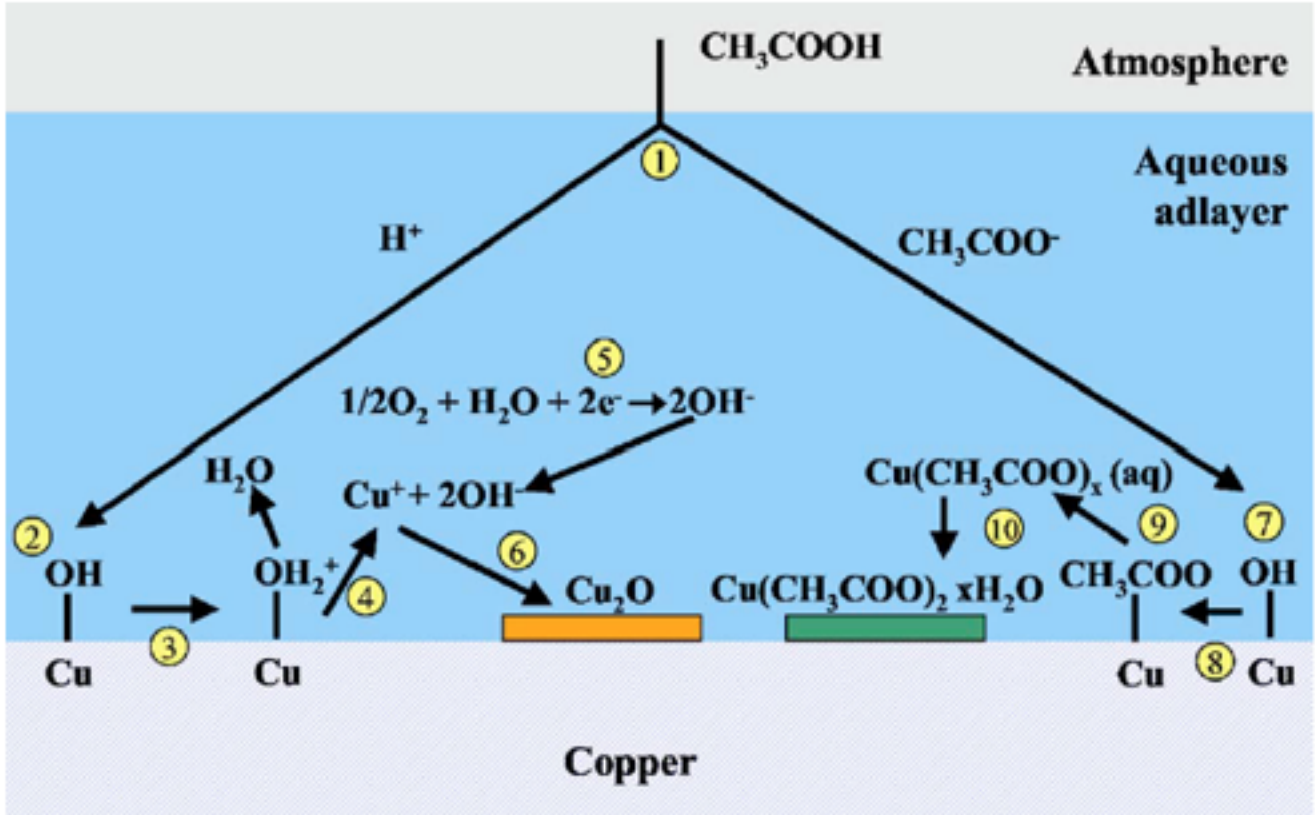
CH3COOH
Atmosphere
Aqueous adlayer
1
H+
CH3COO-
5
1/2O2 + H2O + 2e- → 2OH-
H2O
Cu+ + 2OH-
Cu(CH3COO)x (aq)
2
OH
OH2+
4
6
Cu2O
Cu(CH3COO)2 xH2O
10
9
7
CH3COO
OH
3
8
Cu
Cu
Cu
Cu
Copper

Table 1. *Electrode formulations as prepared with $R_{Cu/COOH}$ molar ratio.*

Wt%	Si	GM15	CMC	CA	Na	K	Cu	SO_4	$R_{Cu/COOH}$
Standard	73.3	11.0	6.7	7.8	0.65	0.64	0	0	0
Cu-0.05	72.3	10.9	6.6	7.7	0.65	0.63	0.50	0.8	0.054
Cu-0.11	71.4	10.7	6.5	7.6	0.64	0.62	0.99	1.5	0.107
Cu-0.21	69.7	10.5	6.3	7.4	0.62	0.61	1.94	2.9	0.214
Cu-0.43	66.5	10.0	6.1	7.1	0.59	0.58	3.70	5.6	0.429

Table 2. *Cu, K and Na quantity in the composition of the matured electrode as a function of the maturation duration, with [Cu] to [COOH in CMC+CA] molar ratio.*

Days of maturation	Na (wt%)	K (wt%)	Cu (wt%)	$\frac{[Cu]}{[COOH]}$
0 (Standard)	0.57	0.68	0.34	0.037
2	0.56	0.61	0.81	0.089
4	0.54	0.62	1.27	0.140
7	0.53	0.62	1.67	0.183

Table 3. *Coulombic efficiency (CE) and irreversible capacity loss at the first cycle and their mean value (at each cycle) between the 2nd and 100th cycle for each sample.*

	Coulombic efficiency (%)		Irreversible loss (mAh g^{-1} per cycle)	
sample	1st cycle	mean value between 2nd and 100th cycle	1st cycle	mean value between 2nd and 100th cycle
Standard	78 ±1	95.6	805	92
Matured 2 days	83 ±1	99.6	643	23
Cu-0.05	82 ±1	99.4	702	26
Cu-0.11	82 ±1	99.4	670	25
Cu-0.21	83 ±1	99.4	622	25
Cu-0.43	86 ±1	99.8	564	19